Scientific Reports

https://doi.org/10.1038/s41598-026-37709-2

Article in Press

Machine learning assisted malaria detection using photonic crystal fibre optical sensors

Received: 29 September 2025

Accepted: 23 January 2026

Published online: 11 February 2026

Cite this article as: Abdullah-Al-Shafi M., Sen S. & Mubassera M. Machine learning assisted malaria detection using photonic crystal fibre optical sensors. *Sci Rep* (2026). https://doi.org/10.1038/s41598-026-37709-2

Mohammad Abdullah-Al-Shafi, Shuvo Sen & Mashiyat Mubassera

Machine Learning Assisted Malaria Detection Using Photonic Crystal Fibre Optical Sensors

Mohammad Abdullah-Al-Shafi[1*], Shuvo Sen[2], Mashiyat Mubassera[3]

[1]Faculty of Science and Engineering, Southern Cross University, Gold Coast, Australia

[2]Department of Information and Communication Technology (ICT), Mawlana Bhashani Science and Technology University (MBSTU), Santosh, Tangail-1902, Bangladesh

[3]QC Analyst II, Ortec Inc, SC, USA

[*]E-mail: alshafi08@gmail.com, m.shafi.11@student.scu.edu.au

Abstract

This study presents a photonic crystal fibre based optical sensor with a simple and practical architecture for malaria detection using refractive index variations in red blood cells. The proposed sensor consists of a hollow central core surrounded by five concentric layers of heptagonal cladding, enabling efficient sample infiltration and enhanced light matter interaction. This configuration provides high sensitivity to subtle refractive index changes while maintaining structural simplicity suitable for real world diagnostic deployment. Refractive index variations corresponding to different Plasmodium developmental stages are converted into distinct wavelength shifts, allowing reliable discrimination between ring trophozoite and schizont stages. The sensor operates over a refractive index range of 1.373 to 1.402, closely matching the optical properties of malaria infected red blood cells. Numerical results demonstrate high relative sensitivity of 97.45 percent for healthy cells, 96.89 percent for the ring stage, 96.22 percent for the trophozoite stage, and 95.45 percent for the schizont stage. Optical confinement losses remain extremely low, on the order of 10^{-8} dB per metre at an operating frequency of 2.2 THz. These results highlight the potential of photonic crystal fibre sensors as a cost effective and high-performance platform for early malaria detection and broader biomedical sensing applications.

Keywords: Photonic crystal fibre, Malaria, Biosensor, Sensitivity, Refractive index, Terahertz.

1. Introduction

Malaria remains one of the most persistent global public health challenges, accounting for millions of new cases each year and emerging as a major factor in illness and death across the world, particularly in tropical and subtropical regions

[1]. The disease is predominantly caused by the protozoan parasite Plasmodium falciparum, which is transmitted to humans through the bite of infected female Anopheles mosquitoes [2]. Upon transmission, the parasite initially migrates to the liver, where it invades hepatocytes and undergoes rapid replication and amplification. Subsequently, merozoites are released into the bloodstream, initiating the intraerythrocytic phase of infection [3]. Within red blood cells (RBCs), P. falciparum progresses through a well-defined sequence of developmental stages, namely the ring, trophozoite, and schizont phases, each marked by distinct morphological and biochemical transformations [4]. The culmination of this cycle involves the separation of the host erythrocyte and the dissemination of newly formed parasites, which continue the infection and give rise to the characteristic cyclic febrile symptoms accompanied by chills, hematological disorders such as anemia, and, in extreme cases, fatal clinical outcomes such as cerebral malaria and multi-organ failure [5].

In 2024, malaria caused an estimated 610,000 deaths worldwide, with an uncertainty range of 561,000 to 738,000 deaths [6]. This represents an increase compared with 2023, when an estimated 598,000 deaths occurred (range: 550,000-725,000) [6]. The rise of approximately 12,000 additional deaths in one year highlights growing challenges in malaria control, particularly in vulnerable settings. When viewed over a slightly longer timeframe, malaria mortality has remained persistently high since the mid-2010s. In 2015, global malaria deaths were estimated at 578,000 (range: 543,000-635,000). By 2020, deaths increased to 621,000 (range: 575,000-736,000), partly due to disruptions in health services during COVID-19 [6]. Although mortality declined after 2020, the level observed in 2024 remains about 32,000 deaths higher than in 2015, indicating that global targets for mortality reduction have not yet been achieved.

In view of the rapid clinical deterioration and the seriousness of its clinical manifestations, timely and reliable diagnostic precision remains a prerequisite for ensuring appropriate therapeutic intervention and to limit fatal outcomes. Nevertheless, widespread disruptions to healthcare systems most prominently observed during the coronavirus respiratory pandemic have substantially impeded the detection, management, and surveillance of multiple infectious diseases, malaria among them [7,8]. These challenges underscore the urgent need for robust, rapid, and highly sensitive diagnostic technologies that can operate efficiently even under constrained healthcare conditions. In recent years, optical sensing approaches, particularly those based on photonic crystal fibre (PCF) technology, have emerged as promising candidates for biomedical diagnostics, including malaria detection [9–11]. PCF-based sensors offer several intrinsic advantages, such as compactness, high sensitivity, minimal reliance on mechanical components, and exceptional flexibility in adjusting core and cladding geometries for targeted sensing applications [12–14]. These attributes have enabled PCFs to demonstrate remarkable performance in the detection of a wide range of biological and chemical biomarkers [15–18].

A fundamental biophysical attribute employed in optical malaria diagnostic approaches is the refractive index (R.I.) of RBCs, which exhibits quantifiable variations as Plasmodium progresses through successive stages of its intraerythrocytic development [19]. The earliest detectable stage of infection, the ring phase, is characterised by the initial establishment of the parasite within RBCs, where it adopts a distinctive ring-shaped morphology readily observable under light microscopy [20]. This stage typically persists for approximately 24 hours and represents a critical window for early diagnosis [21]. As the parasite matures into the trophozoite stage, it exhibits accelerated growth and actively metabolises hemoglobin, leading to pronounced morphological and optical changes within the host cell. This phase generally spans 24-36 hours [21]. The final schizont stage is marked by extensive asexual replication, during which the RBC becomes densely packed with daughter merozoites. Rupture of the erythrocyte follows, releasing merozoites into circulation and triggering the hallmark febrile episodes of malaria. Lasting approximately 36-48 hours, this stage completes the intraerythrocytic cycle and ensures continued disease propagation [21]. Collectively, these highly synchronised and repetitive developmental stages induce significant variations in the optical properties of infected RBCs. Healthy erythrocytes typically exhibit homogeneous R.I. distribution, whereas malaria-infected cells display pronounced spatial irregularities and fluctuations in R.I. due to parasitic growth and intracellular restructuring [19]. These optical contrasts, combined with observable morphological distortions, provide a powerful basis for differentiating between healthy and infected cells [22]. PCF structures with precisely engineered R.I. profiles are therefore uniquely suited for capturing these subtle yet diagnostically significant variations, positioning them as advanced platforms for early and reliable malaria detection. Moreover, the terahertz (THz) spectral band, typically defined over the range of approximately 0.1-10 THz, has gained recognition as a focal area in contemporary clinical and preclinical research due to its pronounced responsiveness to the dielectric, refractive, and electromagnetic properties of biological tissues and compounds. This distinctive interaction capability positions THz waves as a powerful modality for probing subtle structural and compositional variations in biological systems with high precision [23–26].

Building upon recent methodological and technological developments, this study introduces a hollow-core photonic crystal fibre (HC-PCF) sensor personalised for malaria detection, with the aim of achieving heightened sensitivity and improved diagnostic fidelity. The proposed sensor configuration is rigorously conceived and numerically investigated using the Finite Element Method (FEM) within the COMSOL Multiphysics version 5.6 Environment. Finite Element Analysis (FEA) is employed to examine modal interaction and coupling mechanisms within the hollow-core section, facilitating the identification of malaria-associated perturbations through changes in operative R.I., coupling dynamics, and optical propagation responses. Sensor performance is quantitatively assessed by monitoring resonance wavelength shifts in the transmission spectrum, thereby establishing a reliable and high-resolution optical sensing platform for the accurate discrimination of malaria-infected RBCs.

Within the 2.2 THz photonic sensing regime, the sensor reveals consistently strong performance across all developmental phases, exhibiting elevated RS values of 97.45% for the regular phase (n = 1.402), 96.89% for the ring phase (n = 1.395), 96.22% for the trophozoite phase (n = 1.383), and 95.45% for the schizont phase (n = 1.373). Processed concurrently, the corresponding CL stands minimal, observed at 6.09×10^{-8} dB/m for the regular phase, 5.95×10^{-8} dB/m for the ring phase, 5.96×10^{-8} dB/m for the trophozoite phase, and 5.80×10^{-8} dB/m for the schizont phase. This novel framework offers a rapid, robust, and highly accurate strategy for malaria detection, thereby enabling the development of next-generation diagnostic systems with enhanced clinical reliability and translational potential.

2. Conceptual Design and Architectural Framework

To address the growing demand for rapid, label-free, and highly sensitive malaria diagnostics, this research suggests a THz hollow-core PCF sensor specifically designed for R.I.-based detection of malaria-infected RBCs. The sensing concept exploits the strong interaction between the guided THz mode and biologically relevant analytes introduced into the fibre core, enabling subtle pathological variations in RBCs composition to be translated into measurable optical responses. By integrating a heptagonal cladding topology for the THz regime, the proposed design aims to achieve enhanced sensitivity, low confinement loss (CL), and robust operational stability, making it a promising candidate for non-invasive and real-time malaria biosensing applications.

Figure 1 outlines the architectural schematic of the designed heptagonal (H-PCF), incorporating a hollow-core configuration encased by a cladding with heptagonal symmetry. The cladding is formed by five concentric layers of uniformly arranged air holes (AHs), where d_1 denotes the air-hole diameter, and A_1 defines the pitch, measured as the centre-to-centre distance between neighbouring holes. This precisely tailored geometry is optimised to achieve robust modal confinement while preserving mechanical integrity and manufacturability. The hollow core is selectively infused corresponding to infected RBC phases, formed as analyte media with refractive indices of 1.402, 1.395, 1.383, and 1.373, representing distinct stages of pathological progression. The surrounding guiding medium is constructed from Topas polymer, which exhibits a R.I.of 1.5253, as summarised in Table 1. Topas is preferred due to its favourable performance, marked by low absorptive losses and superior thermal and chemical durability, and broad transparency across the THz spectrum. Collectively, these attributes promote enhanced light–matter interaction within the hollow core, following in elevated sensing sensitivity and a pronounced reduction in CL, thereby establishing the proposed H-PCF as a strong candidate for high-performance THz biosensing applications.

The cladding filling fraction, defined by the ratio d_1/A_1, is systematically optimised to achieve an effective trade-off between fabrication practicality and optical performance, consistent with established design principles stated in the research [27,28]. The proposed PCF is specifically designed for well-organised operation across the THz frequency range of 1-3 THz, where strong field confinement and low propagation loss are critical. To further enhance the fibre's performance, comprehensive structural optimisation is conducted using the FEM implemented in the COMSOL Multiphysics environment. A perfectly matched layer (PML) is employed at the outer boundary to absorb outward radiation and eliminate spurious reflections. The PML texture is set to 8% of the most transverse dimension of the fibre, confirming precise modelling of electromagnetic transmission. This numerical framework provides a robust and reliable platform for evaluating the modal characteristics of the proposed design and underpins the validity of the simulated results. The finalised structural parameters, determined through an extensive numerical optimisation framework, comprise a hollow core diameter (d) of 90 μm, a cladding air-hole diameter (d_1) of 345 μm, and a firm cladding pitch of 445 μm across all lattice rings ($A_1 = A_2 = A_3 = A_4 = A_5$). These optimised geometrical specifications are consolidated and reported in Table 2 for clarity and reference.

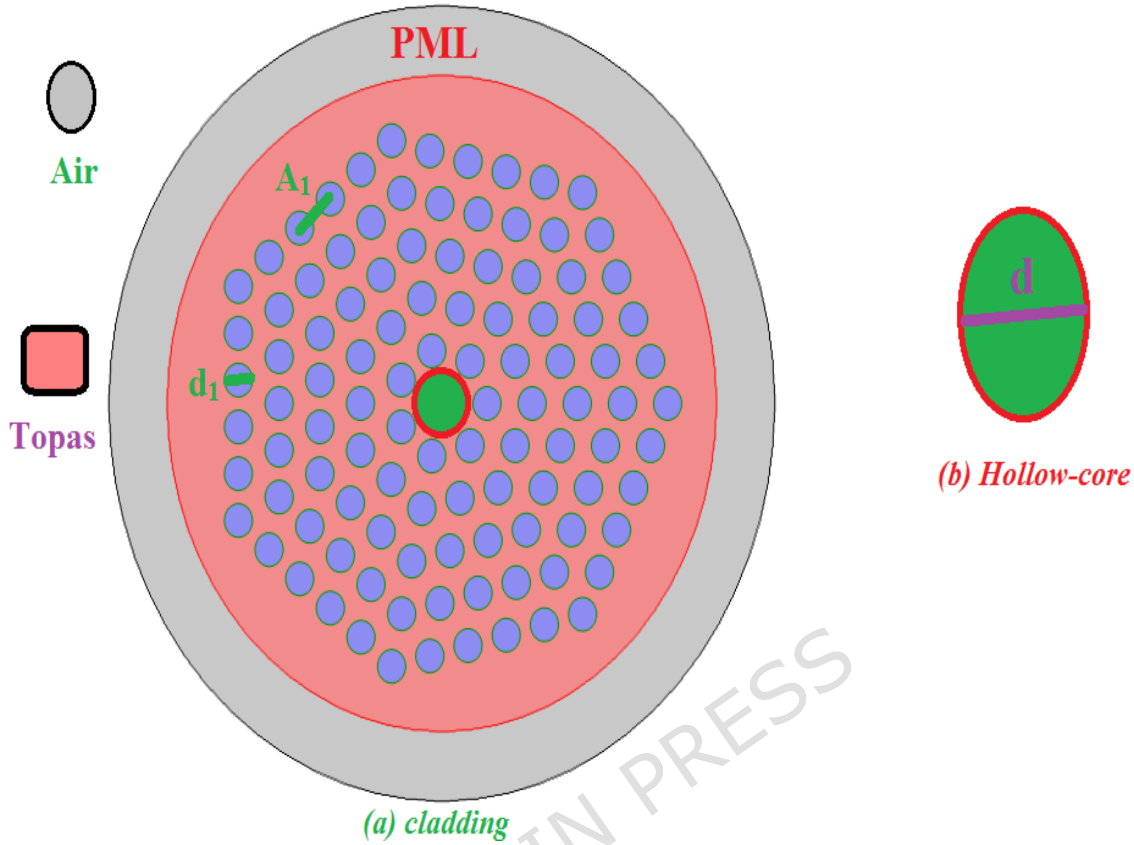

Figure 1: Geometrically symmetric architectures of the designed sensing area: (a) cladding, (b) hollow-core

Table 1: Comparative R.I. characterisation of healthy and infected RBC across progressive malaria stages

RBC levels	R.I.	Research
Non-infected cell	1.402	[29–31]
Cell infected at the ring stage	1.395	
Cell infected at the trophozoite stage	1.383	
Cell infected at the schizont stage	1.373	

Table 2: Comprehensive evaluation of design parameters and performance metrics for the PCF architecture

Characteristics	Measures (μm)	Structures	Valuations

Cladding pitch (A_1)	445	Sensitivity (routine stage)	97.45%
Cladding distance (d_1)	345	Critical functional region (routine stage)	6.85×10^{-8} m^2
hollow core width (d)	90	CL (routine stage)	6.09×10^{-8} dB/m
PML_1	2300	-	-
PML_2	2484	-	-

Figure 2 visualises the power distribution behaviour of RBC samples at an operating frequency of 2.2 THz. The analysis indicates significant confinement of electromagnetic energy concentration in the hollow-core domain, reflecting highly effective field confinement. This concentrated confinement markedly strengthens the coupling between the guided THz wave and the analyte, thereby contributing precisely to the sensitivity enhancement of the proposed sensing platform. Furthermore, Figure 2 includes the corresponding electric-field spatial distributions for selected structural configurations, allowing for an in-depth analysis of the mechanisms governing energy localisation within the sensor architecture. These field distributions clearly demonstrate how the designed geometry promotes effective confinement and controlled propagation of the electromagnetic field, offering critical insight into the physical mechanisms that support the sensor's high-performance response.

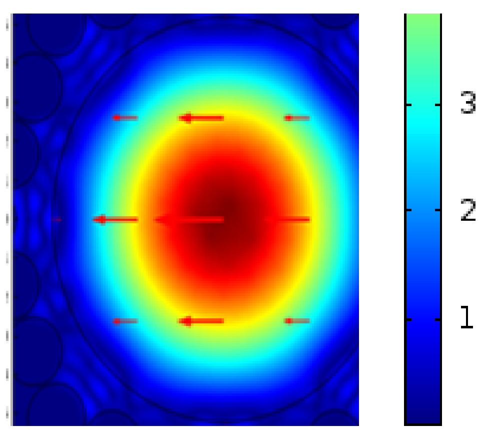

Figure 2. Frequency-Selective energy distribution characteristics at 2.2 THz

To ensure accurate electromagnetic modelling and reliable optical confinement, particular attention was given to boundary treatment and material selection in the proposed sensing architecture. The numerical framework incorporates a PML boundary condition, specifically designed to emulate an open-domain environment by effectively suppressing spurious reflections at the computational edges. The PML is characterised by carefully defined permeability and anisotropic permittivity tensors, which enable efficient absorption of outward-propagating electromagnetic waves. These layers are strategically positioned at the outermost boundary of the structure, thereby ensuring stable field propagation and numerical convergence across the entire simulation domain. Topas polymer was chosen as the structural medium for both the PML and the outer cladding of the detector because of its beneficial optical and mechanical effects. Notably, Topas exhibits strong thermal resilience, minimal effective mode attenuation, and a highly homogeneous R.I. profile. These attributes collectively enhance modal confinement and signal fidelity, thereby rendering the material particularly well-suited for high-precision optical sensing applications. This material choice provides enhanced control over modal behaviour and facilitates fine-tuning of the sensor's optical response. As a result, the overall structural design exhibits strong adaptability across a wide range of advanced purposes, including biological diagnostics, high-speed telecommunication systems, and environmental monitoring platforms [28,32,33].

A key outcome of the parametric investigation is the identification of a pronounced positive correlation between the relative sensitivity (RS) of the device and the air-filling fraction (A_{FF}). This relationship highlights the pivotal influence of symmetrical optimisation on the sensing operation of PCF-based devices. For the present configuration, an A_{FF} value of 0.78 was selected as an optimal compromise, yielding enhanced sensitivity while maintaining mechanical stability. Higher A_{FF} values were deliberately avoided, as excessive air-hole enlargement can lead to structural overlap, compromising fabrication feasibility and undermining the reliability of the photonic crystal lattice. The suggested H-PCF architecture was systematically designed and adjusted using the FEM within the COMSOL Multiphysics environment. A highly refined meshing scheme was implemented to achieve numerical accuracy and stability, consisting of 22,420 triangular domain elements, 3,254 edge elements, and 325 vertex elements. This dense discretisation enables precise resolution of electromagnetic field distributions and modal characteristics. Subsequently, a comprehensive parametric sweep was conducted over a broad operational frequency range to evaluate the sensor's spectral response and performance consistency. To evaluate the real-world feasibility of the proposed sensor for malaria diagnosis, a prototypical experimental setup was designed, as illustrated in Figure 3. In this configuration, a broadband optical source delivers light into a single-mode fibre

(SMF), which is specifically fusion-spliced to the sensing fibre using a Fujikura splicer to minimise insertion and coupling losses [33]. The sensing region undergoes stepwise introduction of analytes with differing refractive indices, representing distinct physiological conditions of RBCs. Before each observation sequence, the sensor probes are rigorously cleansed with deionised water to remove any residual deposits, thereby ensuring measurement integrity and eliminating the risk of cross-contamination between samples.

When RBC samples engage with ligand-functionalised interfaces in the active sensing zone, subtle but detectable variations in the optical transmission spectrum are induced. These spectral modulations are taken through the SMF and precisely resolved with an optical spectrum analyser (OSA). The ensuing spectral information is then relayed to a computational platform for advanced post-processing and analytical interpretation, enabling accurate extraction of transmission signatures characteristic of malaria-infected RBCs. This integrated detection workflow enables high-resolution optical interrogation and accurate discrimination of infection stages, thereby demonstrating the strong diagnostic capability of the proposed sensor. Figure 3 further presents the triangular meshing configuration employed in the numerical model, emphasising the geometric arrangement of the photonic crystal structure. The generation of periodic air-hole patterns within the PCF cladding using this mesh framework is essential for controlling key optical phenomena, including modal confinement, field diffusion, and selective mode propagation. Such specific structural engineering allows the optical response to be deliberately tailored, ensuring optimal performance across a diverse range of sensing and photonic applications [34–36].

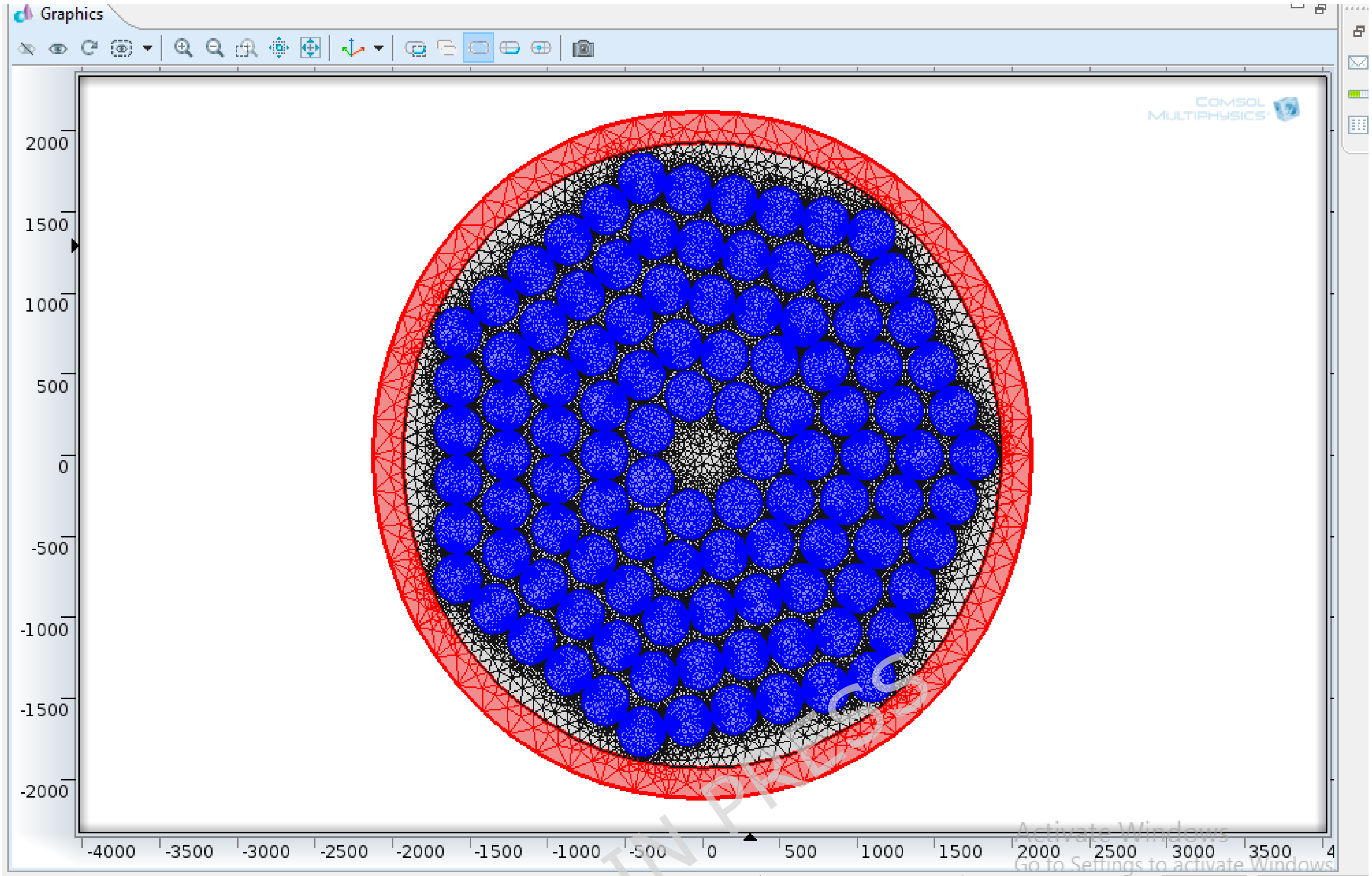

Figure. 3: A mesh-resolved schematic illustrating a computationally optimised architecture with an implicit hollow-core configuration

3. Sensor Configuration and Experimental Methodology

Figure 4 illustrates the experimental arrangement adopted to realise and assess the optimised PCF sensor, which has been purposefully developed for malaria detection. This configuration is conceived to ensure efficient light-matter interaction while maintaining compatibility with standard fibre-optic instrumentation. By integrating conventional optical components with a carefully engineered PCF architecture, the setup provides a robust and reproducible platform for evaluating the sensing capability of the designed sensor under controlled circumstances. The overall system consists of a broadband laser source, an SMF, and an OSA. Light emitted from the source is first guided through the SMF via a coupling, ensuring stable and well-defined mode excitation before entering the sensing region. The guided optical signal is then launched into the HC-PCF, where the presence of the analyte enables strong evanescent-field interaction within the core. The heptagonal cladding geometry surrounding the hollow core plays a pivotal role in adjusting light confinement and enhancing sensitivity. To comprehensively assess the identification capability of the sensor, this PCF configuration has been systematically simulated for a range of malaria-related substances, allowing performance variations to be quantitatively analysed.

After propagating through the PCF, the transmitted light is collected at the output end and directed to the OSA, where wavelength-dependent spectral characteristics are recorded with high resolution. These spectral signatures are subsequently transferred to an information-processing unit for detailed evaluation, including resonance shifts and intensity variations associated with different analytes. Such a processing pipeline enables precise discrimination of malaria indicators based on their optical response. The upper portion of Fig. 4 provides a cross-sectional representation of the HC-PCF, offering insight into its internal microstructured geometry. The cladding comprises a periodic arrangement of AH forming a heptagonal lattice, designed to regulate modal propagation and field distribution. At the centre lies the hollow core, which serves as the primary sensing region. Key functioning factors, such as the diameter (d) and pitch (Λ), are explicitly indicated, as these dimensions critically influence CL, sensitivity, and overall sensor performance. Additionally, a PML is implemented around the PCF boundary in the numerical model to suppress spurious reflections and ensure accurate simulation results. Collectively, this configuration delivers a comprehensive depiction of both the optical signal flow and the operational attributes essential for achieving cutting-edge malaria sensing.

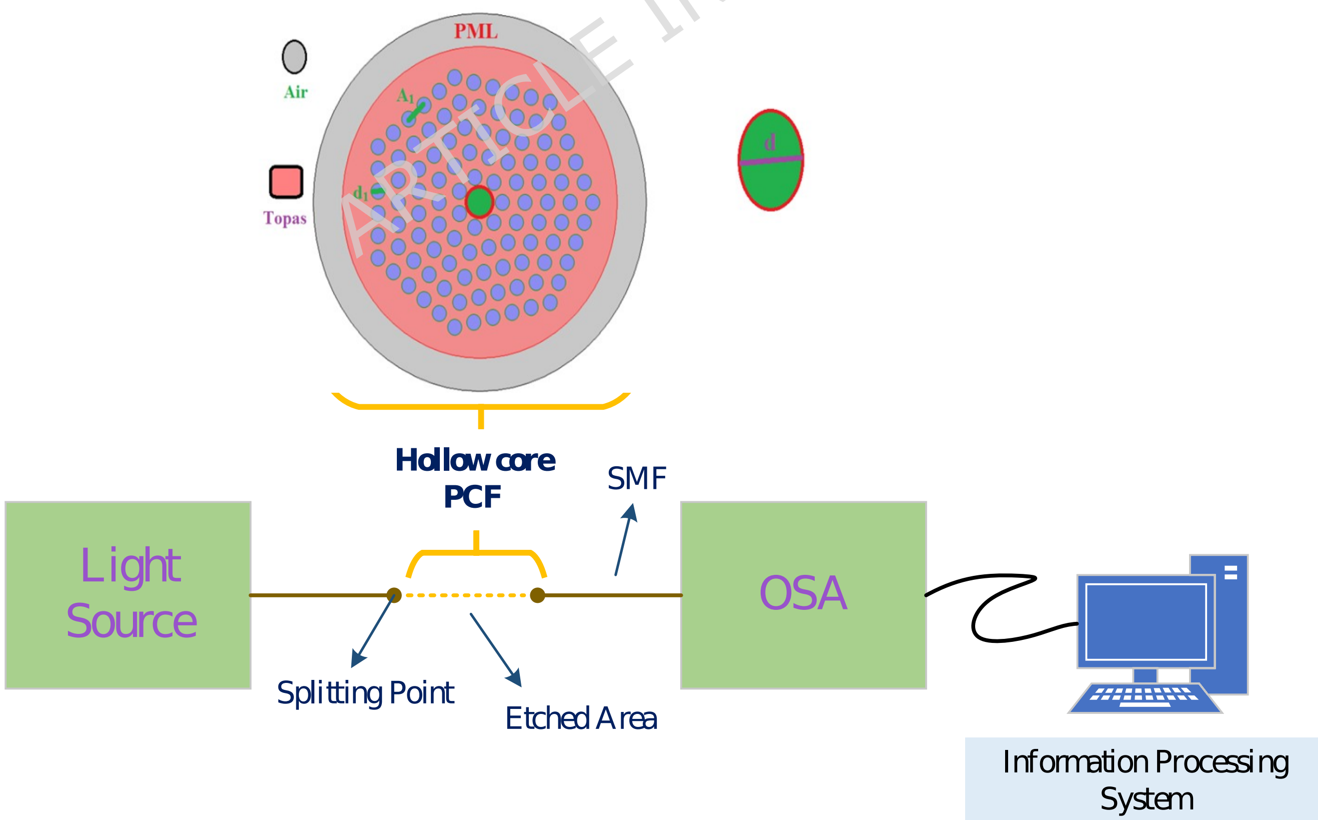

Figure 4. Graphic representation of the validation framework for the PCF-based optical sensing platform

4. Performance Evaluation, Results, and Critical Discussion

A comprehensive numerical framework was established to rigorously analyse the electromagnetic behaviour of the proposed sensor. At the outset, a full-wave computational approach was adopted to capture the intricate field interactions that govern wave propagation within microstructured optical fibres operating in the THz domain. FEA was employed to solve Maxwell’s equations with high fidelity, enabling accurate characterisation of the spatial distribution of electromagnetic fields and the associated wave–matter interactions. By discretising the complex fibre geometry into a finite number of smaller elements, this method allows the contribution of each structural component to be evaluated with precision, thereby offering deep insight into the underlying sensing mechanisms. All numerical simulations were implemented using COMSOL Multiphysics, which provided a robust platform for investigating the core sensing features of the designed PCF architecture. Particular attention was devoted to the comprehensive assessment of the effective mode area (A_{eff}), RS, EML, and CL, as these interdependent parameters collectively govern the functional efficiency of the proposed sensor. To ensure a physiologically representative modelling framework within the THz regime, RBC states were employed as the target analytes, with numerical simulations performed across a wide spectral range of 1-3 THz. Building upon this baseline analysis, plasmodium-positive samples were subsequently unified into PCF architecture to validate the sensor’s applicability in biomedical diagnostics. The influence of pathological alterations on critical performance indicators, including sensitivity, CL, EML, and effective modal characteristics, was rigorously assessed and benchmarked against the healthy RBC scenario. The investigation commenced with a detailed evaluation of the sensor’s relative sensitivity, establishing a foundational reference point for determining its detection efficacy and overall analytical reliability.

The sensing efficacy of PCFs is primarily dictated by their RS, which provides a quantitative indication of the extent to which the photonic characteristics react to external stimuli. These stimuli may include changes in R.I., applied pressure, or temperature fluctuations, and the magnitude of RS directly reflects the fibre’s capability to transduce such perturbations into measurable optical signals [37]. Because of their microstructured geometry, PCFs generally exhibit substantially higher sensitivity than conventional optical fibres, as the guided optical mode experiences a more substantial overlap with the surrounding or infiltrated medium [23]. The interaction between guided light and the surrounding medium significantly heightens the fibre’s ability to detect subtle environmental perturbations. Importantly, the RS of a PCF is not a fixed material property; instead, it emerges from a complex interplay of factors such as the functional wavelength, the architectural layout of the air-hole lattice, and ambient external influences. As a result, the sensing performance of PCF-based platforms can be strategically engineered through accurate geometric optimisation, positioning them as highly versatile and powerful tools for high-precision sensing applications. In the present study, the RS was calculated using the formulation (1), reported in [24], which provides a reliable basis for evaluating and comparing the sensing efficiency of PCF-based biosensors.

$$RS = (P / n\_r) \times 100 \quad (1)$$

In this formulation, n_r refers to a model-dependent parameter related to R.I. sensing. The parameter P denotes the fractional optical power, as evaluated according to Equation (2) [24].

$$P = \frac{\int_{sample} R_e(E_x H_y - E_y H_x) dxdy}{\int_{total} R_e(E_x H_y - E_y H_x) dxdy} \quad (2)$$

The electromagnetic power distribution associated with malaria-related substances at different developmental phases, namely the normal (healthy) state, ring state, trophozoite state, and schizont state, was systematically examined. The investigation focused on their electromagnetic responses by analysing the x-component of the magnetic field intensity (H_x) and the x-component of the electric field (E_x). Under x-polarised conditions, these field components exhibit equivalent behaviour, allowing a consistent basis for comparative evaluation across all stages.

Figure 5 depicts the RS response of the designed R.I. sensor corresponding to distinct stages of plasmodium-positive blood within the THz frequency domain. The response of the sensing architecture was systematically estimated over a broad spectral range from 1 to 3 THz. Throughout this interval, the detector exhibits a stable and progressive improvement in sensitivity as the operating frequency increases, reflecting the favourable interaction between the guided THz waves and the analyte. A pronounced optimum is observed at 2.2 THz, where the sensor delivers its highest sensitivity levels. At this frequency, the RS attains 97.45% for healthy (normal) blood, while values of 96.89%, 96.22%, and 95.45% are recorded for the principal erythrocytic stages (ring, trophozoite, schizont), respectively. The gradual yet discernible reduction in sensitivity with disease progression underscores the sensor’s strong discriminatory capability. Overall, these findings demonstrate the proposed detector’s robustness and precision in resolving subtle R.I. variations associated with different malaria stages, thereby confirming its strong potential for high-fidelity biomedical diagnostics within the THz range.

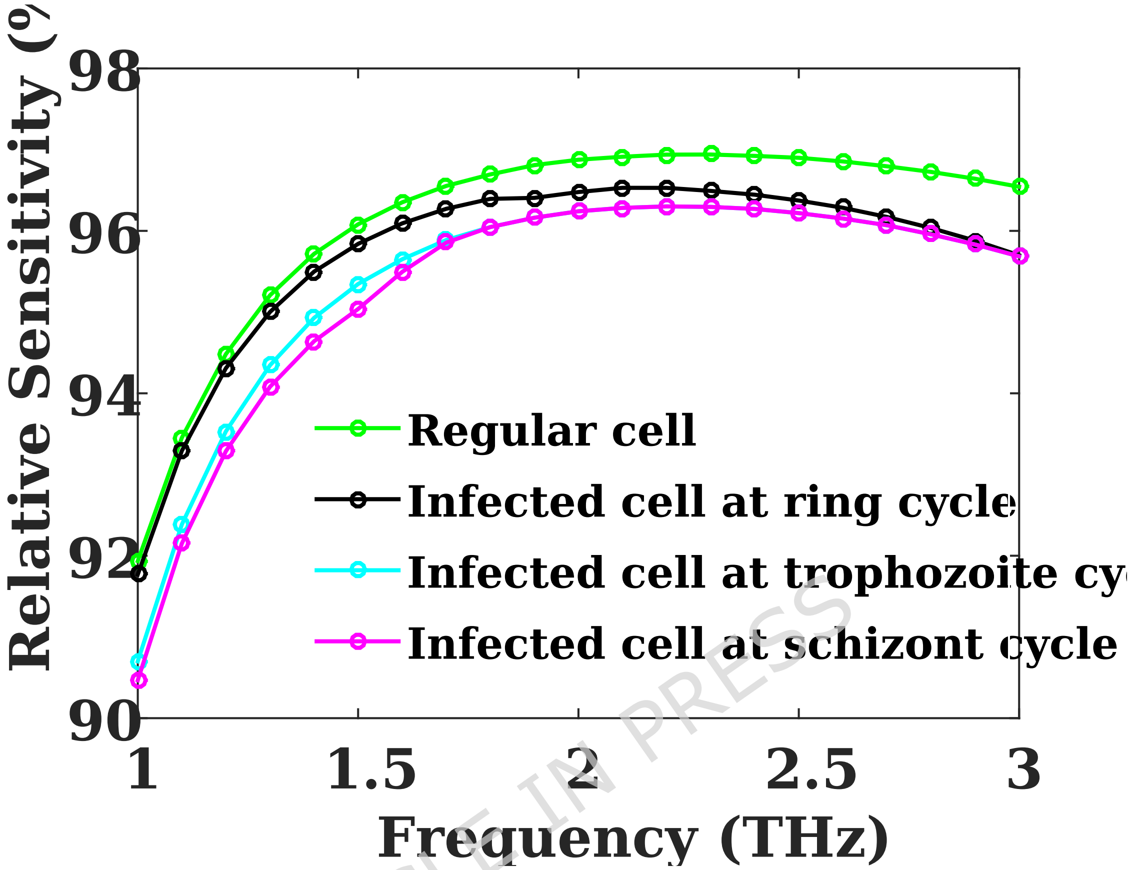

Figure 5: Frequency-Responsive behaviour of RS

In optical fibre-based systems, efficient light guidance relies on the ability of the waveguide to confine electromagnetic energy within its core over extended propagation lengths. However, perfect confinement is fundamentally unattainable, and a fraction of the optical power inevitably escapes into the surrounding regions as light travels along the fibre [38]. This gradual attenuation of optical intensity arises from the partial extension of the evanescent field beyond the core-cladding boundary and constitutes an intrinsic limitation of waveguide-based photonic structures. The resulting phenomenon, commonly referred to as CL, acts as a decisive character in defining the transmission efficiency, constancy, and sensing capability of fibre optic devices. In the context of PCF sensors, CL is a particularly critical performance metric, as it directly governs the strength of light-matter interactions and, consequently, the achievable sensitivity and measurement fidelity. CL may originate from multiple sources, including unavoidable structural irregularities introduced during fabrication and enhanced coupling between guided modes and the surrounding environment. Such loss mechanisms can severely impair sensor accuracy, especially in high-precision or ultra-sensitive detection applications. Accordingly, any rigorous assessment of PCF sensor performance must explicitly account for CL alongside other key optical parameters.

Beyond intrinsic waveguide effects, additional attenuation can arise from system-level leakage mechanisms, often linked to imperfect structural design or misalignment of auxiliary features such as breath vents [33]. These imperfections can further facilitate unwanted energy dissipation, thereby compounding the overall loss. Within the PCF architecture, the presence of air-filled microstructured voids acts as non-conductive regions that enable strong light guidance while suppressing excessive interaction with the surrounding medium. The careful optimisation of these hollow regions is therefore essential for minimising loss and enhancing device performance. Quantitative evaluation of CL in PCF sensors is achieved by methodically tuning the fibre's symmetrical configuration and structural composition, followed by rigorous electromagnetic analysis. In particular, CL is derived from the complex components of the effective R.I., in conjunction with the EML, which collectively capture both radiative leakage and absorption-related effects. The detailed mathematical formulation (3 and 4) underpinning this approach is well established in the literature and is comprehensively described in [39].

$$CL = 8.686 \times k0 \times \mathrm{Im}(n\_eff) \quad (3)$$

$$k0 = 2\pi\left(\frac{f}{c}\right) \quad (4)$$

In Equation (4), the electric-magnetic field oscillation is parameterised by its operating wave rate (f) and its phase velocity, taken as the speed of light in free space ($c = 3 \times 10^8\ ms^{-1}$). The operator Im extracts the imaginary component of the complex wave function, which encodes the oscillatory and phase-dependent characteristics of the electromagnetic field, capturing the phase-related behaviour of the field. Conversely, in Equation (3), k0 represents the parameter associated with spontaneous wave excitation, serving as a fundamental descriptor of the wave generation mechanism.

Figure 6 delineates the dependence of CL on THz frequency, offering valuable insight into the guiding behaviour and operational efficiency of the proposed fibre under optimised conditions. As the frequency increases, a pronounced reduction in CL is observed, reflecting progressively improved mode confinement and more efficient light guidance within the fibre structure. This trend indicates that higher-frequency THz waves are more effectively confined, thereby minimising energy leakage. Notably, within the 2-3 THz interval, the CL profile exhibits a quasi-steady response with only marginal fluctuations, highlighting the structural stability and reliable performance of the fibre across this operational bandwidth. Such frequency-independent behaviour is particularly advantageous for sensing applications, as it ensures consistent signal propagation and measurement of fidelity. At a characteristic frequency of 2.2 THz, the fibre reveals its most favourable confinement characteristics, yielding minimum CL values of 6.09 × 10^{-8} dB/m for the regular phase, 5.95 × 10^{-8} dB/m for the ring phase, 5.96 × 10^{-8} dB/m for the trophozoite phase, and 5.80 × 10^{-8} dB/m for the schizont phase. These exceptionally low loss values underscore the fibre's strong potential for high-precision THz wave detection and reinforce its suitability for advanced sensing and diagnostic applications.

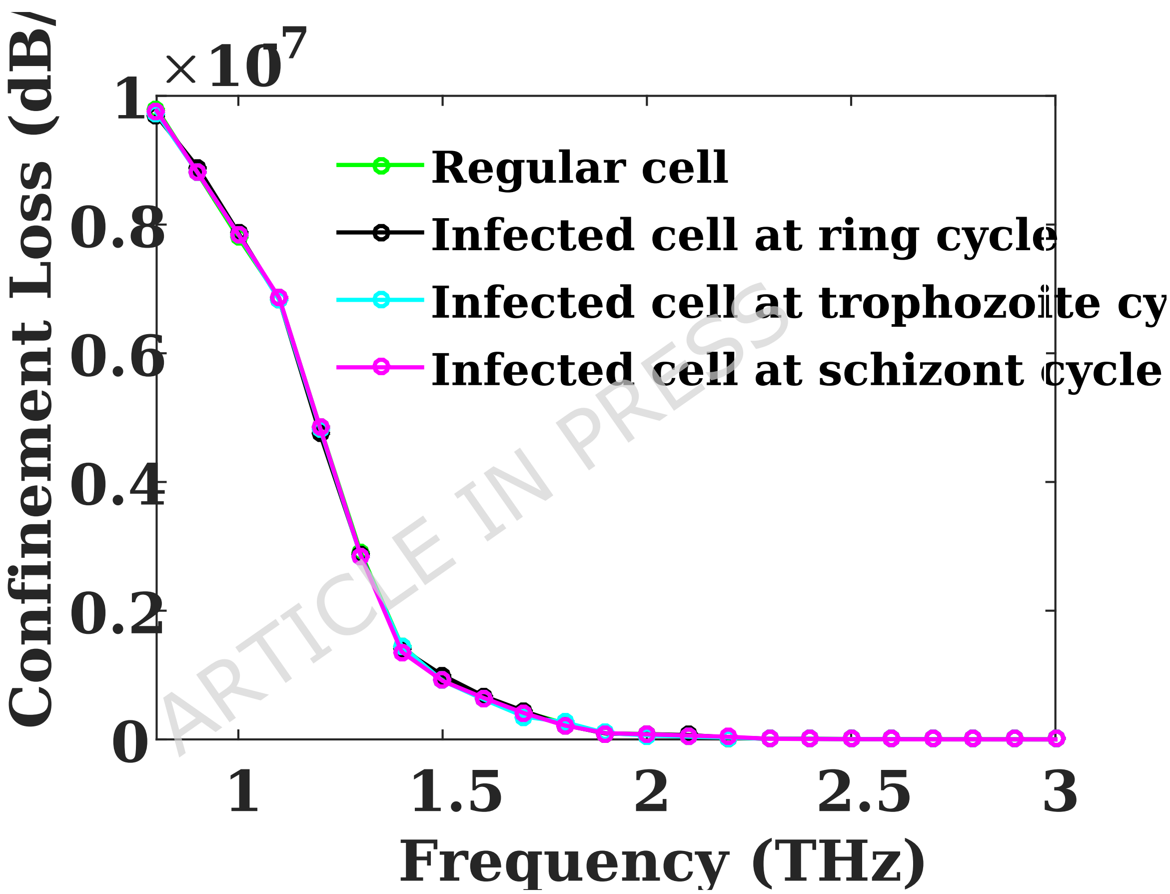

Figure 6: Systematic evaluation of frequency-driven CL across all developmental phases-regular, ring, trophozoite, and schizont, highlighting phase-specific propagation characteristics

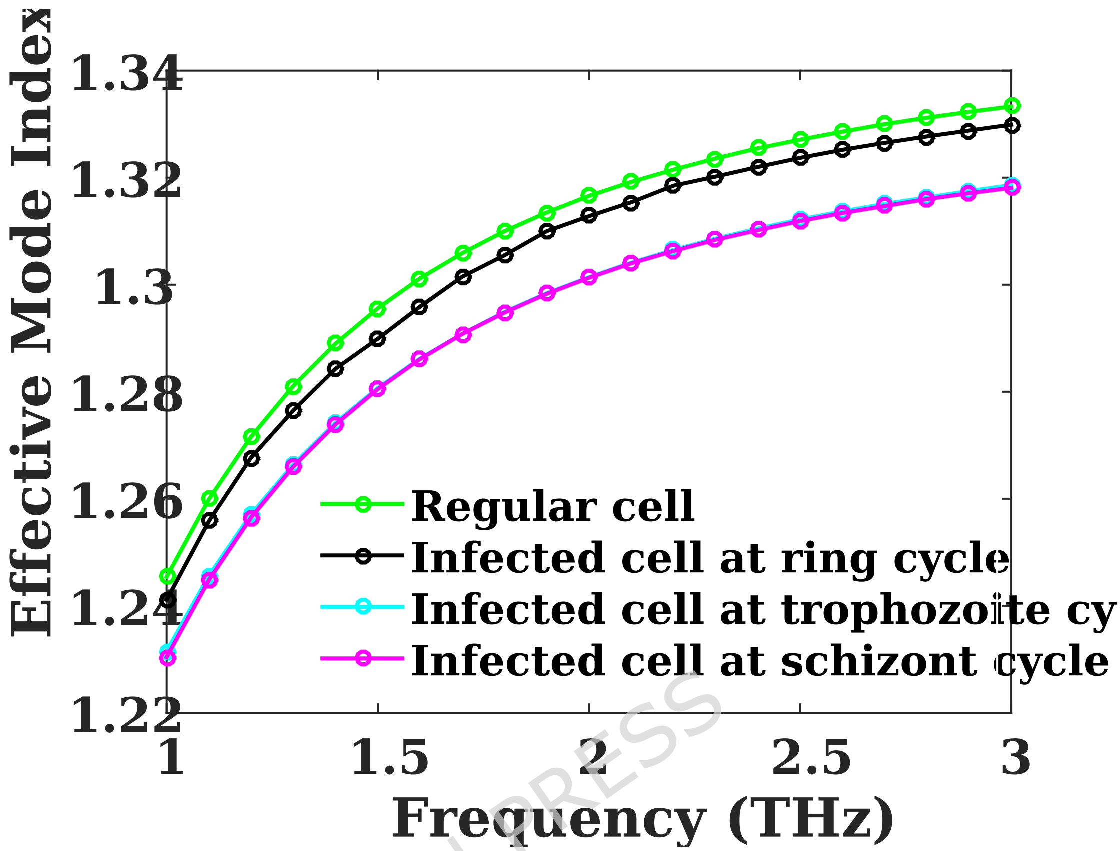

Figure 7: Comprehensive analysis of the effective refractive mode index over an extended frequency spectrum, highlighting its progressive variation throughout all stages in comparison with the normal condition

Figure 7 exhibits an inclusive exploration of the effective mode index (EMI) as a mapping of frequency, offering deeper insight into the modal dynamics of the proposed structure under biologically relevant conditions. By systematically examining the response across the THz spectrum, this figure explains how electromagnetic confinement and propagation characteristics evolve for all the stages, thereby establishing a clear link between frequency modulation and stage-dependent optical behaviour. At the lower end of the spectrum, the EMI attains its minimum value of approximately 1.24 at 1 THz, indicating comparatively weaker modal confinement. With increasing frequency, the EMI increases in a gradual and monotonic manner, reaching a maximum value of about 1.32 at 3 THz, which reflects enhanced field localisation and improved guiding efficiency. Notably, a pronounced resonance-like anomaly is observed near 2.2 THz, signifying a critical transition point in the periodic modal response and underscoring the complex interaction between the guided mode and the structural dispersion characteristics.

A clear distinction among the biological stages is evident in the EMI values, further emphasising the sensitivity of the system to subtle material variations.

Specifically, the regular stage reveals the peak EMI of approximately 1.31, subsequently the ring stage at 1.30, the trophozoite stage at 1.29, and the schizont stage at 1.28. This orderly reduction in EMI across stages highlights the frequency-dependent nature of modal propagation and demonstrates the competence of the designed platform to discriminate between different stages obtained from their electromagnetic signatures. Collectively, these observations confirm the strong potential of the structure for advanced THz waveguiding and stage-specific sensing applications. An essential metric for assessing the energy transport performance of a PCF is the power fraction, a factor that measures the distribution and confinement of optical power within the guiding region. This characteristic has been rigorously analysed and well documented in the literature (Equation 5), notably by **[26]**.

$$P = \iint\_core \, Re(E \times H^*)\cdot\hat{z} \, dA \, / \iint\_total \, Re(E \times H^*)\cdot\hat{z} \, dA \qquad (5)$$

In this work, the numerator is evaluated by integrating over the individual structural domains, namely the core region, the surrounding cladding, and the embedded air cavities. The total optical power across the fibre cross-section is then obtained by summing the corresponding contributions appearing in the denominator, thereby yielding a comprehensive representation of the power distribution.

Figure 8 demonstrates the periodicity-dependent behaviour of the power fraction across the regular, ring, trophozoite, and schizont phases in a benchmark device setting. At an operating frequency of 1 THz, the power fraction originates at a relatively modest magnitude, reflecting limited coupling efficiency at shorter periodic intervals. As the periodicity is progressively increased, a consistent and monotonic enhancement in the power fraction is observed for all developmental stages, indicating a stronger interaction between the propagating field and the structured medium. This upward trend persists across the examined range and ultimately converges toward a pronounced peak at 3 THz, where the device exhibits its highest power confinement and transfer efficiency. Such behaviour underscores the critical role of periodicity in optimising spectral performance and highlights its influence on stage-dependent power distribution within the proposed architecture. This monotonic enhancement highlights a strong dependence of power confinement on periodic modulation across all developmental stages. At the resonant frequency of 2.2 THz, the experimentally obtained power fraction shows remarkably elevated values through all developmental phases, reaching 97.60% for the regular stage, 97.03% for the ring stage, 96.80% for the trophozoite stage, and 96.70% for the schizont stage.

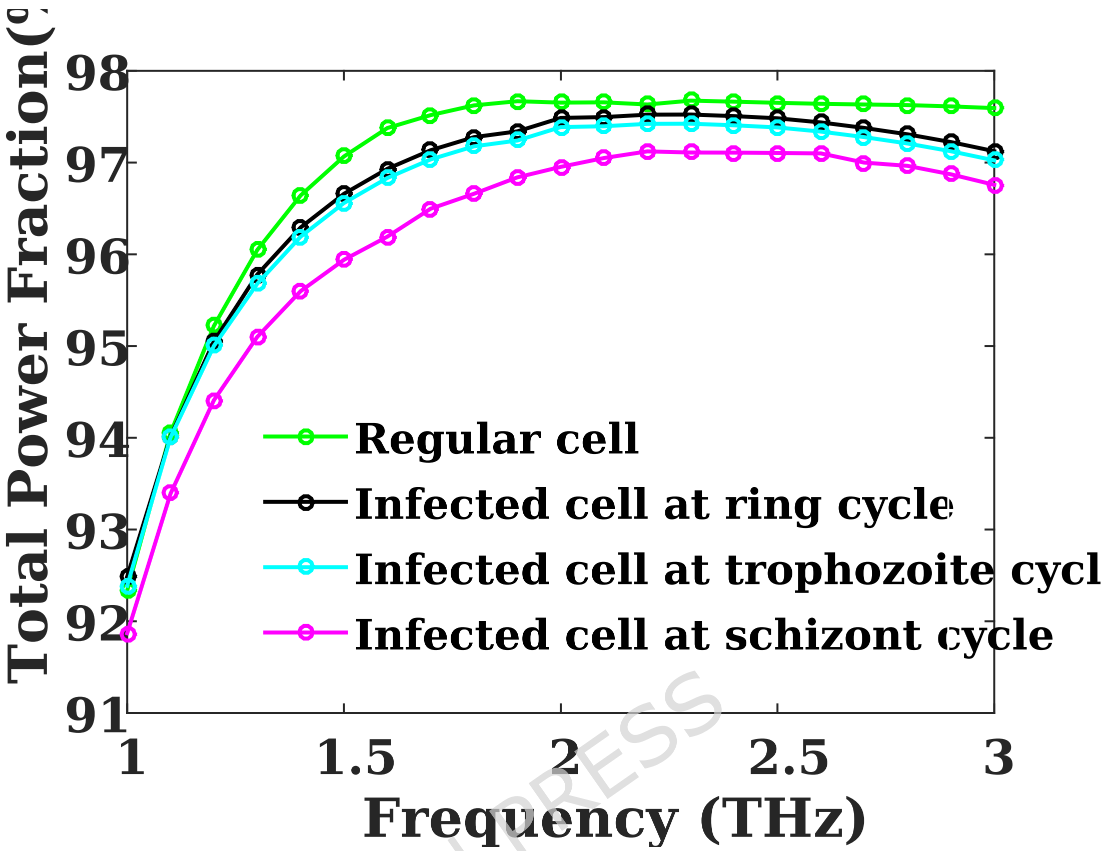

Figure 8: Frequency-dependent distribution of optical power fraction across all stages

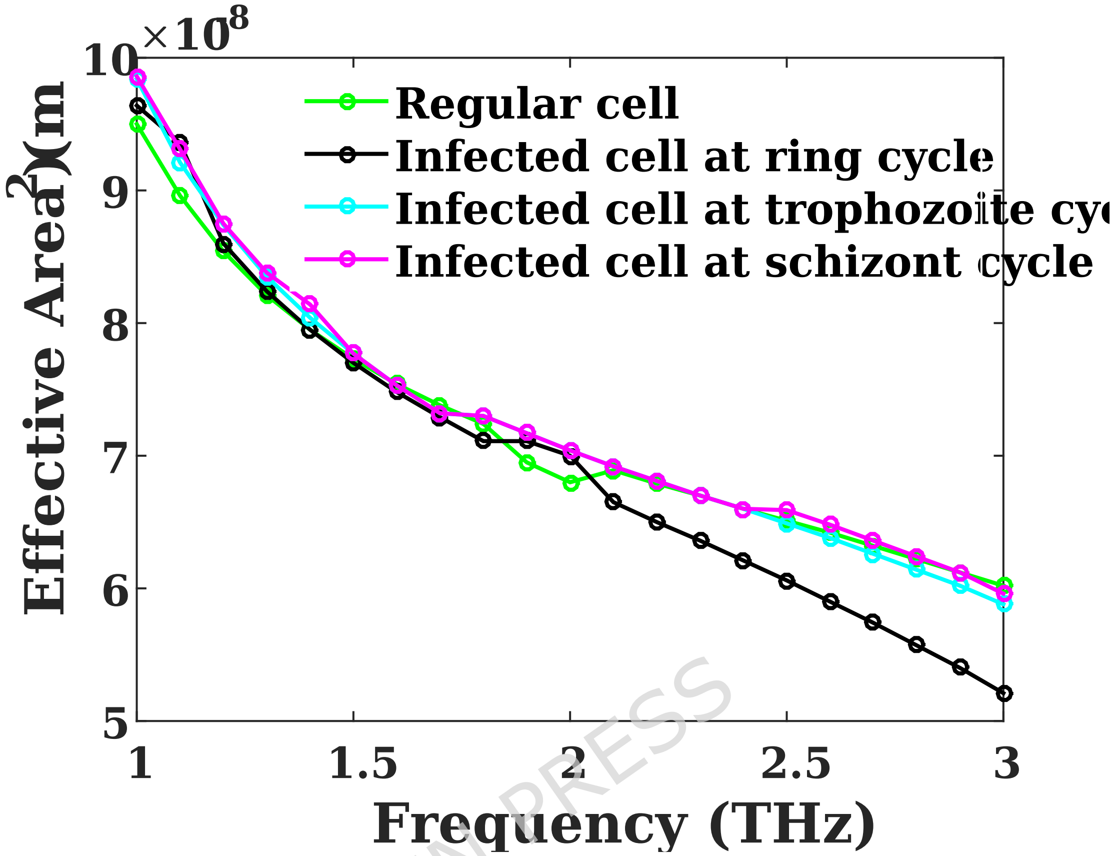

Figure 9: Frequency-dependent variations in the A_{eff} distinctly characterise all stages, revealing stage-specific optical responses across the investigated spectrum

A_{eff} is a fundamental parameter in fibre optics, as it directly governs optical confinement, nonlinear interactions, and overall device sensitivity. A precise understanding of this quantity is therefore essential for evaluating and optimising fibre-based sensing and detection platforms. In the context of advanced photonic structures, variations in A_{eff} often reflect subtle changes in modal distribution and light–matter coupling, providing valuable insight into the functional behaviour of the fibre. In this work, the A_{eff} of the proposed sensor fibre is systematically examined to elucidate its underlying guiding characteristics. Physically, A_{eff} represents the cross-sectional region over which the photonic intensity of a specific guided mode is disseminated inside the fibre. It characterises the spatial footprint of the propagating laser field, effectively describing how the electromagnetic energy is spread across the fibre's transverse plane. In this sense, A_{eff} serves as a quantitative measure of modal confinement, indicating the degree to which optical energy is localised within the core region. PCFs, due to their highly organised microstructured cladding, exhibit distinctive light-guiding mechanisms that arise from a combination of spectral bandgap effects and total internal reflection. This complex geometry enables exceptionally strong confinement of the guided mode, typically yielding a markedly reduced A_{eff}

compared with that of conventional step-index fibres. Such a reduction in A_{eff} significantly enhances light-matter interaction, intensifies field overlaps with the sensing region, and improves the overall performance of PCF-based devices. A comprehensive theoretical and numerical behaviour of A_{eff} (Equation 6) analysis is available in the work of **[24]**.

$$A_{eff} = \left(\iint |E|^2 \, dA \right)^2 / \iint |E|^4 \, dA \quad (6)$$

In this formulation, $\left(\iint |E|^2 \, dA \right)^2$ encapsulates the cumulative contribution of the transverse intensity distribution, whereas $\iint |E|^4 \, dA$ quantifies the absolute optical power sustained inside the system. The characteristic spatial reach of the radiative field is thus directly implied from the limits over which this allocation remains significant. Notably, A_{eff} emerges as a pivotal parameter governing wave transport, as it directly modulates modal confinement, propagation efficiency, and the strength of light-matter interactions within the waveguide architecture.

Figure 9 illustrates the dependence of the PCF effective area on the operating frequency, demonstrating a pronounced and orderly inverse relationship between these two parameters. As the frequency is progressively increased, a systematic reduction in the effective area is observed, indicating an intrinsic trade-off that constrains system performance at higher spectral regimes. This trend emphasises that frequency selection is not merely a design choice but a decisive factor governing the operational optimisation and functional stability of the PCF sensor. Notably, at a working frequency of 2.2 THz, the sensor exhibits a distinctly outlined effective area, reflecting robust confinement characteristics and stable sensing behaviour. At this frequency, the effective area attains values of 6.85×10^{-8} m² for the regular phase, 6.70×10^{-8} m² for the ring phase, 7.20×10^{-8} m² for the trophozoite phase, and 7.30×10^{-8} m² for the schizont phase. These findings indicate that the design is capable of sustaining high performance across biologically relevant stages within this spectral window. Overall, the observed frequency-dependent behaviour highlights the strong coupling between spectral modulation and sensing performance in PCF-based platforms. Precise modulation of the operating frequency directly influences light-matter interaction, thereby dictating the accuracy, reliability, and overall effectiveness of signal acquisition in advanced photonic sensing applications.

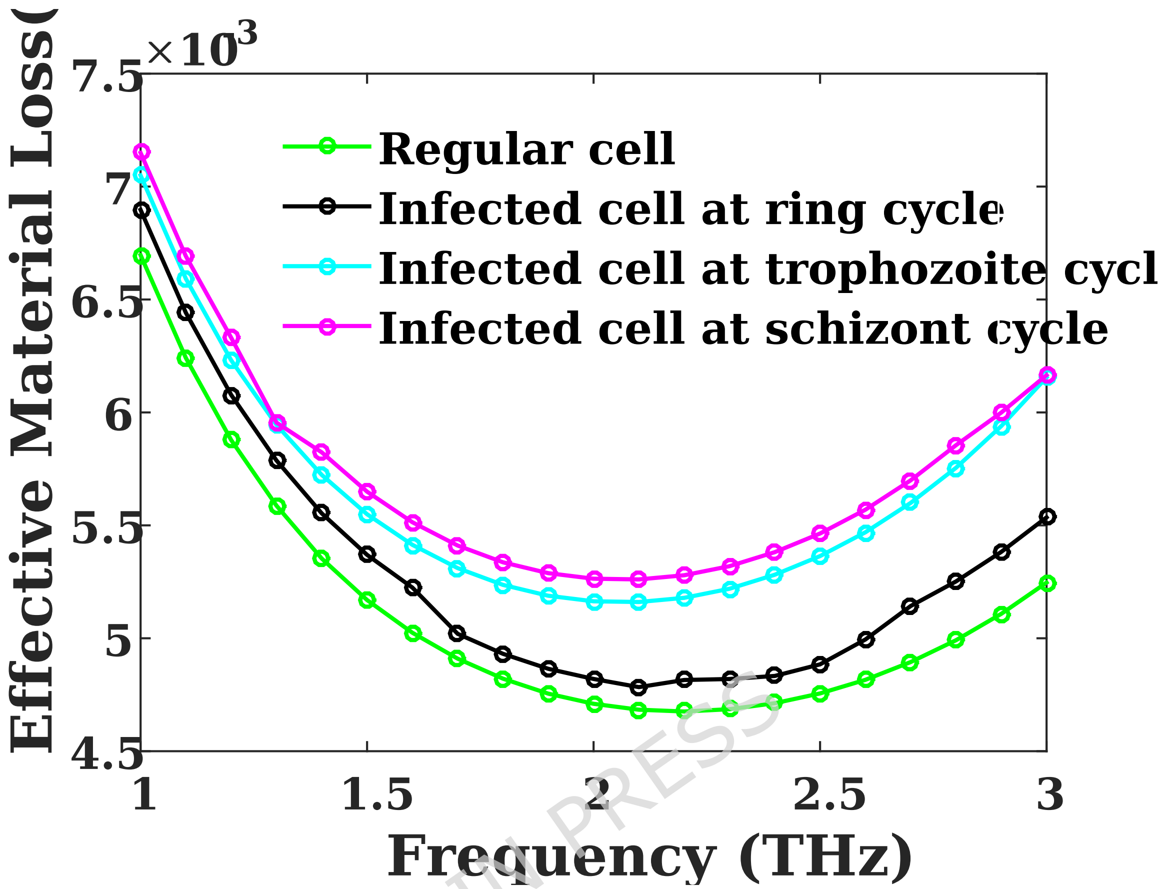

Figure 10: Variation of A_{eff} with frequency for regular and parasitic developmental phases, including Ring, Trophozoite, and Schizont

Optical loss mechanisms portray a decisive part in supporting the efficiency and reliability of PCF sensing platforms. A comprehensive understanding of these losses is therefore indispensable for optimising wave-matter interactions and enhancing overall sensor performance. In practical waveguide structures, losses are unavoidable and arise from both material absorption and imperfect confinement of the guided mode [40]. In this context, the sensor is primarily influenced by two intrinsic loss components, namely CL and EML. Among the various loss contributions in THz wave propagation, EML emerges as the dominant attenuation mechanism, as it directly characterises the fraction of electromagnetic energy confined within the fibre core that is ultimately dissipated through material absorption. In contrast CL, which primarily arises from the leakage of guided modes into the surrounding environment, EML offers a more physically representative measure of power dissipation occurring within the guiding region itself. Precise regulation of these loss processes is therefore critical for the realisation of fibre-based sensing platforms that demand high sensitivity and minimal signal degradation. In practical terms, EML accounts for the gradual decay of optical power along the propagation path as the guided THz field interacts with both the core and cladding microstructure, resulting in a significant decline in transmitted intensity. Attenuation behaviour is strongly governed by the essential electromagnetic properties of the constituent materials, as well as by the physical layout of the PCF, including the R.I. profile, modal confinement efficiency, and spatial overlap between the propagating mode and lossy regions of fibre architecture. Consequently, EML serves as a critical performance metric for evaluating and optimising THz PCF sensor designs. The mathematical expression (Equation 7) directing EML is formulated as follows [30]:

$$EML = (\alpha / 2) \times \left(\iint\_{material} |E|^2 \, dA \, / \iint\_{total} |E|^2 \, dA \right) \tag{7}$$

This formulation enables a precise quantification of directional power transport and provides a robust theoretical basis for analysing energy transmission and loss mechanisms within the electromagnetic framework.

Figure 10 illustrates the dependence of EML on diverse structural and functional configurations over the investigated THz frequency spectrum. The analysis clearly demonstrates a pronounced trend: EML progressively diminishes with increasing core dimensions. This observed trend emphasises the decisive influence of core geometric configuration on attenuation behaviour, demonstrating that structural optimisation can substantially suppress material-related losses, particularly at larger core dimensions. By carefully modifying the fibre architecture, the adverse impact of intrinsic absorption is effectively alleviated, thereby enhancing overall transmission performance across the operational bandwidth. Notably, the proposed sensor fibre achieves exceptionally low EML, reaching a minimum of 2.2 THz. In quantitative terms, this corresponds to attenuation coefficients of 0.00656 cm^{-1} for the normal stage, 0.00612 cm^{-1} for the ring stage, 0.00710 cm^{-1} for the trophozoite stage, and 0.00721 cm^{-1} for the schizont stage. These consistently low loss values across all developmental stages underscore the robustness of the fibre design and highlight its strong potential for high-sensitivity, low-loss biosensing applications. These results demonstrate that the reduction of EML is of vital importance, as diminished attenuation directly improves the sensor’s sensitivity, measurement fidelity, and operational robustness. The analysis further confirms that rigorous control of EML constitutes a decisive factor in enabling high-accuracy and reliable THz sensing performance.

Birefringence is an essential phenomenon of anisotropic optical media, highlighting a wide range of polarisation-sensitive photonic applications. A rigorous examination of birefringence is therefore indispensable for the rational design and optimisation of PCF sensing platforms, especially in environments where external perturbations can significantly modulate optical behaviour. In anisotropic materials, birefringence emerges when electromagnetic waves propagate along non-equivalent optical axes, experiencing distinct refractive indices as a function of their polarisation state [41]. In this work, the birefringent response of the PCF is systematically investigated under immersion in a range of malaria-infected biological media, encompassing the regular, ring, trophozoite, and schizont stages.

Here, birefringence is quantitatively determined using Equation (8), following the formulation reported by [30], which characterises the R.I. asymmetry along the two mutually orthogonal major axes. This formulation enables a precise assessment of optical anisotropy arising inside the PCF. To explain the relations between the guided photonic modes and the surrounding biological setting, the PCF is immersed in media representative of different malaria infection stages. The corresponding changes in birefringence are then examined in detail. These responses stem from the coupled influence of the fibre's microstructured architecture and the R.I. properties of the external medium, which collectively modulate modal confinement and propagation. As a result, distinct alterations in polarisation behaviour are observed, providing a sensitive optical signature of the surrounding biological environment. The analysis reveals the sensitivity of birefringence to subtle environmental perturbations, highlighting its utility as a robust indicator of fibre-medium interactions. The insights gained from this investigation are of particular significance for applications demanding precise polarisation control, where even marginal R.I. fluctuations in the surrounding medium can induce pronounced changes in optical performance. Moreover, the findings advance the fundamental understanding of PCF interactions with complex biological substances and provide practical guidance for adjusting fibre architectures for high-sensitivity biosensing and THz photonic functions.

$$B = |n_x - n_y| \tag{8}$$

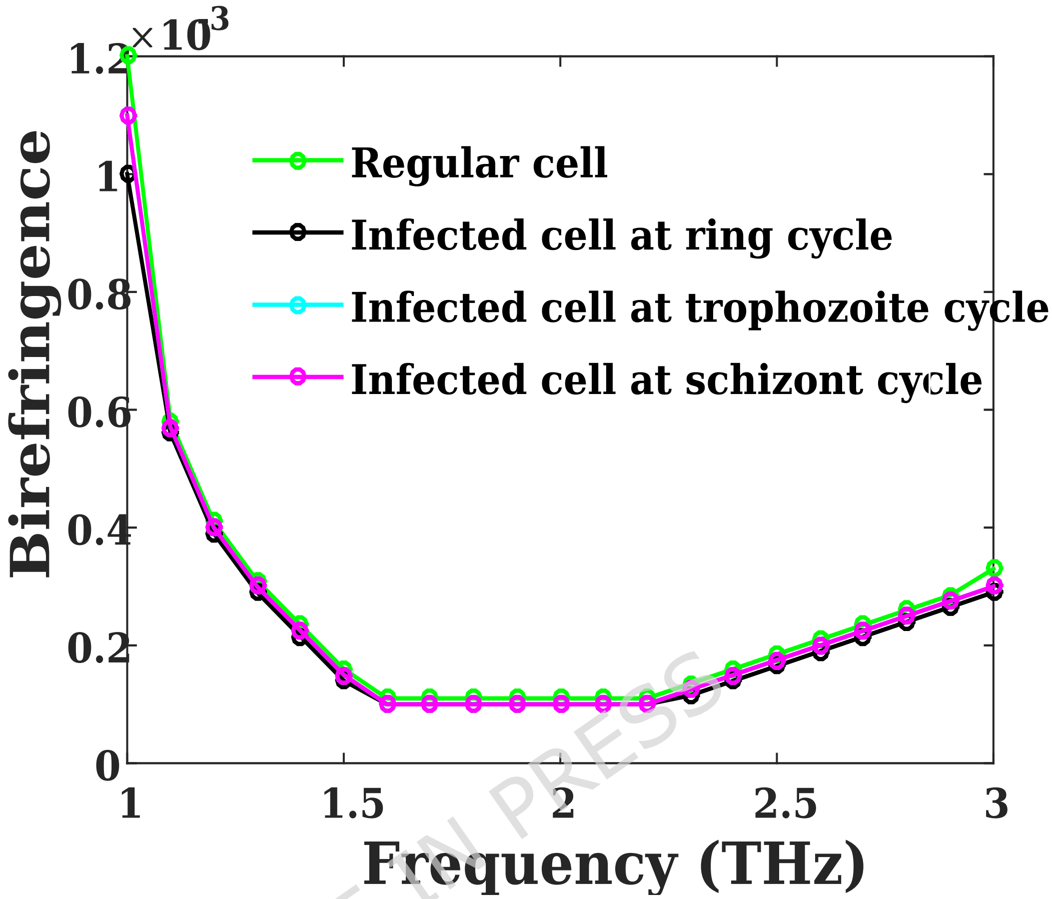

Figure 11: Frequency-dependent birefringence characteristics of malaria parasite developmental stages

Figure 11 presents the birefringence characteristics of the designed PCF-based malaria cell detection platform across the THz frequency domain. The fibre's optical response was comprehensively analysed over the 1-3 THz range to elucidate its behaviour within this technologically and biologically relevant spectral region. This frequency span allows a rigorous evaluation of the dispersion-driven evolution of birefringence, offering insight into the sensor's ability to respond to subtle perturbations arising from variations in the surrounding medium. At an optimal operating frequency of 2.2 THz, all examined stages of malaria infection exhibited birefringence values on the order of 1.1×10^{-3}. Although modest in magnitude, this birefringence reflects a well-defined anisotropy between the effective refractive indices along the two orthogonal polarisation axes of the fibre. Such clearly discernible optical asymmetry highlights the strong light-matter interaction enabled by the engineered PCF geometry and confirms its responsiveness to parasite-induced modifications in the local R.I. environment. Importantly, the ability to resolve these small birefringence variations demonstrates that the proposed PCF architecture is sufficiently sensitive to differentiate between malaria-infected cell stages based on minute R.I.

contrasts. The uniform and repeatable birefringence trends observed across all cell types further attest to the structural stability and measurement reliability of the fibre. Collectively, these findings establish the proposed sensor as a robust and high-precision platform, capable of exploiting subtle optical anisotropies for reliable malaria detection within the THz regime.

The present investigation proposes a comprehensive assessment of the frequency-dependent behaviour of the sensor, with precise highlighting of its interaction with malaria-infected media. A well-structured modulation of the optical response is perceived across the investigated frequency range, reflecting the complex coupling mechanisms between the guided electromagnetic field and the anisotropic biological environment. This behaviour manifests as pronounced variations in key optical characteristics, highlighting the sensitivity of the fibre architecture to subtle adjustments in the neighbouring medium. Importantly, the results reveal that birefringence plays a central role in governing this interaction, significantly enhancing the sensor's discrimination capability. By exploiting this birefringence-induced contrast, the proposed THz-based sensing platform achieves improved precision and selectivity, thereby reinforcing its suitability for advanced biomedical diagnostics. In addition to performance evaluation under ideal environments, the robustness of the designed hollow-core sensor has been systematically assessed by introducing ±2% variations in the optimised structural parameters. This tolerance analysis focuses on critical optical metrics, including RS and CL, which are essential indicators of sensing efficiency and signal integrity. As summarised in Table 3, the induced variations in RS and CL remain marginal when compared with the values obtained for the optimised configuration, indicating a high degree of structural stability. Such resilience against minor fabrication inaccuracies is particularly advantageous, as it simplifies the manufacturing process while maintaining consistent sensor performance. Consequently, the adoption of the optimised design parameters not only ensures operational robustness but also enhances the practicality of large-scale fabrication. Taken together, the results confirm that the designed sensor architecture exhibits strong suitability for practical, real-world applications, with significant promise for industrial and biomedical applications that require accurate and reliable chemical and biological detection.

Table 3: Effect of ±2% Parameter variations on RS and CL at 2.2 THz

Indicators (%)	**RS (%)**	**CL (dB/m)**
	Routine phase	**Routine phase**
+ 2 %	97.95%	6.65×10^{-8} dB/m

ARTICLE IN PRESS

Peak performance	97.45%		6.09×10^{-8} dB/m	
-2 %	95.98%		5.85×10^{-8} dB/m	

Table 4 provides a comprehensive benchmark valuation of the sensitivity achieved by the proposed THz sensor in comparison with a range of state-of-the-art THz sensing platforms previously reported in the literature [39,42–48]. The performance characteristics of multiple THz sensors are critically examined and collectively synthesised to reveal prevailing trends, relative strengths, and distinguishing features across different design approaches. To ensure a fair and transparent comparison, key performance indicators are organised in a structured and standardised manner, accompanied by clearly defined analytical formulations. This systematic presentation facilitates a rigorous assessment of sensing capability and highlights the comparative advantages of the proposed sensor within the broader THz sensing landscape [39,44,47,49,50].

Table 4: Quantitative sensitivity assessment of the proposed and reference structures

Research by	Design	Frequency regime	RS (%)	CL (dB/m)	EML (c/m)
[48]	D-shaped PCF with micro-rectangular opening. Hexagonal lattice of air holes (3 rings)	1285 - 2950 nm	------	9190.0	------
(Ferdous et al., 2023)	An elliptically contoured core embedded within a rectangular cladding matrix	2.80 THz	80.34	------	0.034
(Iqbal et al., 2020)	A circular core encircled by air inclusions arranged in a heptagonal symmetry	2.00 THz	91.50	$1.51{\times}10^{-12}$	0.0072
(Hossain & Sen, 2021)	A rotationally offset heptagonal core integrated into a hexagonally ordered lattice	1.00 THz	68.48	$2.13{\times}10^{-9}$	------

(Islam et al., 2018)	A Kagome-inspired framework incorporating elongated rectangular air voids	1.60 THz	85.70	1.7×10^{-9}	------
(Habib et al., 2021)	A cylindrical core surrounded by circular air holes distributed in a hexagonal configuration	1.94 THz	82.52	1.5×10^{-10}	----------
(Jibon et al., 2021)	A cladding architecture comprising a square central cavity complemented by multiple rectangular elements	1.90 THz	92.70	3.78×10^{-12}	0.0064
[42]	Hexagonal lattice of air holes (2 layers). Gold-coated over circular surface	698 - 936 nm	------	293.0	------
Designed sensor	A hollow core embedded in a heptagonally arranged cladding domain	2.2 THz	97.45	6.09×10^{-8}	0.00656

Fabrication strategies are fundamental to the evolution and performance enhancement of optical sensor architectures, as they directly influence structural precision, reproducibility, and functional reliability. Over the years, literature has documented a diverse spectrum of mature and emerging fabrication approaches, each offering distinct advantages depending on the targeted sensing application. These include mechanical drilling methods that enable precise geometric control, sol-gel synthesis routes known for their compositional flexibility and material uniformity, capillary stacking techniques that facilitate complex microstructured arrangements, and the extensively adopted stack-and-draw process, which remains a cornerstone for producing high-quality optical structures at scale. Collectively, these methodologies emphasise the continued innovation of advanced optical sensors by enabling tailored design, scalable production, and enhanced light-matter interaction characteristics. Among these, the sol-gel approach has gained increasing attention due to its operational simplicity, cost-effectiveness, and strong compatibility with sensor-oriented PCF designs **[51–53]**. In parallel, selective filling has emerged as a highly efficient strategy for introducing analytes directly into the PCF core region, enabling precise material infiltration while preserving the fibre's structural integrity **[54–57]**. When combined in a coherent manner with an optimised structural configuration, these fabrication approaches provide a high degree of control over critical waveguiding characteristics, including RS, CL, A_{eff}, power overlap, and modal effective index. Such precise regulation of guiding behaviour enables systematic enhancement of light-matter interactions within the sensing region, thereby significantly elevating overall sensor performance. As a result, the proposed design framework not only advances sensitivity and operational robustness but also strengthens the practical viability of the sensor for real-world biomedical diagnostic applications.

5. Practical Implementation and Real-World Applicability

Recent advances at the intersection of photonic sensing and data-driven intelligence have opened new avenues for next-generation biomedical diagnostics. In particular, the convergence of optical fibre technologies with advanced computational learning paradigms is redefining how biological signals are acquired, interpreted, and translated into clinically actionable outcomes. Within this context, the incorporation of sophisticated machine learning (ML) strategies with PCF-based architecture has emerged as a compelling and rapidly evolving research direction, offering substantial promise for improving the sensitivity, reliability, and speed of disease detection [52]. The unique structural attributes of PCF enable precise manipulation of modal confinement, dispersion, and evanescent field distribution, thereby allowing for highly sensitive interrogation of biological specimens [51]. These attributes are especially beneficial for the interrogation of complex biological media, such as whole blood, in which subtle alterations in R.I. or optical absorption properties may provide early and sensitive signatures of emerging pathological states [53]. In the case of malaria, subtle optical signatures associated with the presence and progression of Plasmodium parasites can be captured through PCF-based transmission or spectral responses. Nevertheless, the rich optical outputs generated by PCF sensors are inherently high-dimensional, nonlinear, and often contaminated by noise arising from biological variability and experimental conditions. Extracting diagnostic-relevant information from these heterogeneous datasets, therefore, demands advanced analytical frameworks that extend well beyond conventional signal processing techniques [58].

ML, and meta-learning in particular, offers a robust solution to these challenges by enabling adaptive and data-efficient model development. Model-Agnostic Meta-Learning (MAML) has emerged as a prominent meta-learning framework, distinguished by its capacity to identify a highly effective parameter initialisation that enables swift adaptation to previously unseen tasks. By employing only a limited set of task-specific samples, MAML facilitates rapid fine-tuning while preserving strong generalisation performance, making it particularly well-suited for data-scarce learning scenarios [56]. When applied to PCF-based malaria diagnostics, MAML facilitates the construction of predictive models capable of generalising across diverse patient cohorts, blood compositions, and environmental settings. This adaptability is especially critical in real-world healthcare scenarios, where annotated biomedical datasets are often limited and costly to obtain. By significantly reducing the amount of task-specific retraining required, MAML not only enhances predictive accuracy under data-scarce conditions but also lowers computational overhead, making it well-suited for practical diagnostic deployment [57].

Concurrently, integrated deep learning frameworks that adjoin convolutional neural networks (CNNs) with recurrent paradigms, most notably long short-term memory networks, substantially enhance the system's capacity to model complex patterns, capture temporal dependencies, and deliver more robust analytical performance [59]. CNNs excel at automatically learning discriminative spatial and spectral features from PCF transmission profiles, capturing subtle patterns linked to parasitic infection. Meanwhile, LSTM networks are adept at modelling temporal dependencies and dynamic signal variations, such as those arising from the temporal evolution of parasite development stages within blood samples [60]. The incorporation of attention mechanisms into these hybrid frameworks enhances both performance and interpretability by highlighting the most informative spectral bands or temporal segments contributing to classification decisions. This level of transparency is of paramount importance for clinical translation, as it fosters trust in algorithmic predictions and provides insights into the underlying biophysical mechanisms.

Beyond algorithmic performance, the integration of PCF sensors with ML-driven analytics paves the way for compact, portable, and real-time diagnostic systems suitable for patient-side applications. By employing a decentralised computational paradigm and optimised ML architectures, on-device inference can be achieved without reliance on cloud infrastructure [61]. This capability enables immediate diagnostic feedback, minimises delays associated with sample transportation, and broadens access to reliable testing in remote or resource-limited environments. Moreover, progress in few-shot learning and transfer learning extends the versatility of the platform, allowing rapid adaptation to the detection of multiple infectious diseases beyond malaria using limited additional data screening [62].

In summary, the convergence of PCF-based optical sensing technologies with sophisticated ML methodologies, particularly meta-learning strategies such as MAML, introduces a powerful and forward-looking paradigm for precision diagnostic systems. This interdisciplinary integration capitalises on the exceptional optical sensitivity, structural flexibility, and controllable light-matter interaction of PCFs, while simultaneously leveraging the learning efficiency, adaptability, and transparent decision-making capabilities of advanced ML frameworks. The resulting synergy facilitates the design of diagnostic systems that are not only rapid and reliable but also resilient to data scarcity and variability across clinical settings. Beyond its immediate relevance to improving malaria detection accuracy and responsiveness, this approach provides a versatile and scalable foundation for next-generation optical fibre-based biosensors. As such, it holds considerable promise for advancing precision medicine, enabling early disease identification, and supporting global health initiatives through cost-effective and deployable diagnostic solutions. A schematic flowchart illustrating the malaria detection pipeline incorporating MAML, transfer learning, and LSTM architectures is presented in Figure 12.

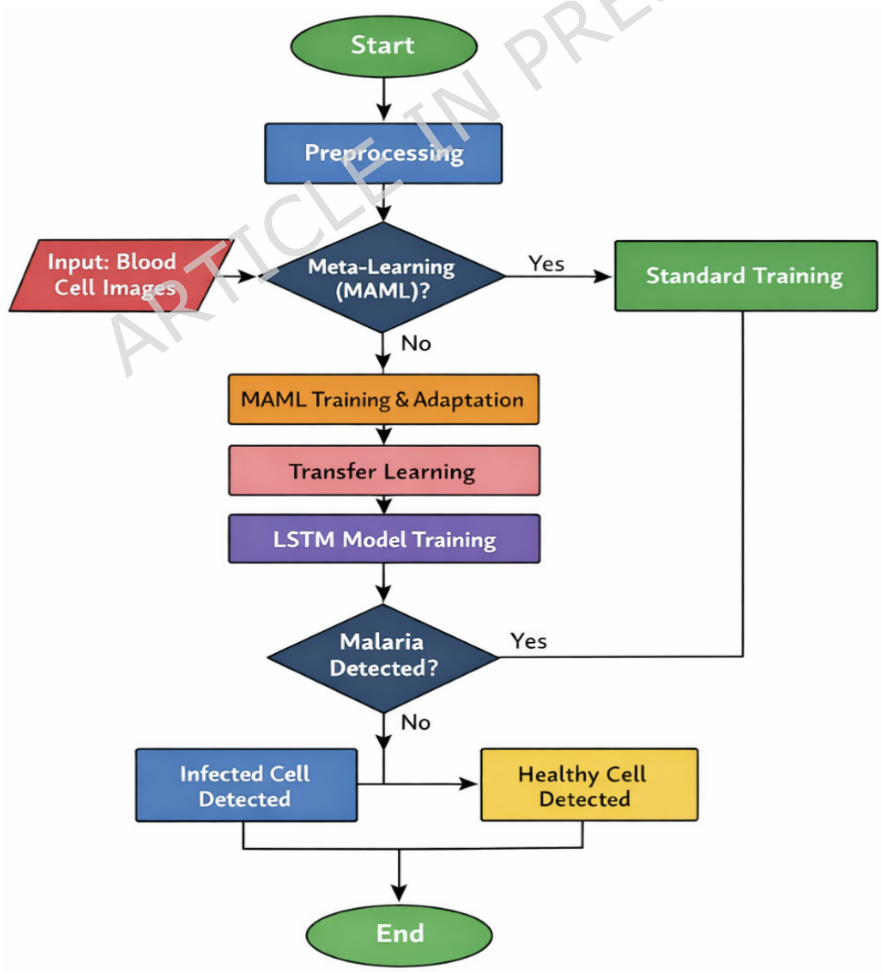

Figure 12: Conceptual pipeline for robust malaria diagnosis through MAML-

driven adaptation, transfer learning, and LSTM sequence analysis

6. Conclusion

This research proposes an advanced malaria detection methodology employing a PCF-based biosensing platform, thoroughly analysed through FEM simulations conducted in the COMSOL Multiphysics environment. The sensing mechanism is predicated on quantifying resonant peak wavelength shifts in the transmission spectrum arising from R.I. variations between healthy and malaria-infected RBC. To enhance sensing performance, key geometrical and optical parameters of the PCF, including air-hole arrangement, pitch, and analyte infiltration region, were systematically optimised. Detailed numerical results reveal pronounced wavelength displacement corresponding to progressive stages of malaria infection, yielding exceptionally high sensitivity and strong spectral distinguishability. These outcomes emphasise the capability of the designed sensor to achieve accurate, stage-resolved malaria detection with robust optical responsiveness and high diagnostic reliability. Precisely, under X- polarised excitation, the sensor demonstrates consistently robust sensitivity across all malaria phases. Specifically, sensitivities of 97.45%, 96.89%, 96.22%, and 95.45% are achieved for the regular, ring, trophozoite, and schizont phases, respectively. Correspondingly, the associated confinement losses remain extremely marginal, considered at 6.09×10^{-8} dB/m for the regular phase, 5.95×10^{-8} dB/m for the ring phase, 5.96×10^{-8} dB/m for the trophozoite phase, and 5.80×10^{-8} dB/m for the schizont phase, all evaluated at a sensing frequency of 2.2 THz. Collectively, these results emphasise the outstanding sensing capability of the proposed architecture, which surpasses the performance of existing designs and establishes it as a robust and substantially effective approach for precise and reliable stage-specific detection.

Data Availability: No datasets were generated or analysed during the current study.

Acknowledgements: The authors would like to thank the anonymous reviewers for reviewing the paper.

Funding: Not available.

Authors Contributions:

Mohammad Abdullah-Al-Shafi: Conceptualisation, Data curation, Formal analysis, Investigation, Writing - original draft.

Shuvo Sen: Methodology, Resources, Software analysis, Validation, Visualisation.

Mashiyat Mubassera: Methodology, Investigation, Resources, Visualisation

Declarations

Ethics Approval: Not applicable.

Consent to Participate: The authors agreed to submit the paper to this journal.

Consent for Publication: The authors provide consent for publication.

Competing Interests Statement: The authors declare no competing interests.

References

1. Kogan, F. Malaria Burden. in *Remote Sensing for Malaria: Monitoring and Predicting Malaria from Operational Satellites* (ed. Kogan, F.) 15–41 (Springer International Publishing, Cham, 2020). doi:10.1007/978-3-030-46020-4_2.
2. Habtamu, K., Petros, B. & Yan, G. Plasmodium vivax: the potential obstacles it presents to malaria elimination and eradication. *Trop. Dis. Travel Med. Vaccines* **8**, 27 (2022).
3. Aly, A. S. I., Vaughan, A. M. & Kappe, S. H. I. Malaria Parasite Development in the Mosquito and Infection of the Mammalian Host. *Annu. Rev. Microbiol.* **63**, 195–221 (2009).
4. Djokic, V., Rocha, S. C. & Parveen, N. Lessons Learned for Pathogenesis, Immunology, and Disease of Erythrocytic Parasites: Plasmodium and Babesia. *Front. Cell. Infect. Microbiol.* **11**, 685239 (2021).
5. White, N. J. Malaria parasite clearance. *Malar. J.* **16**, 88 (2017).
6. World Health Organisation. World malaria report 2025. https://www.who.int/teams/global-malaria-programme/reports/world-malaria-report-2025 (2026).
7. Abdullah-Al-Shafi, Md. COVID-19 pandemic: a viewpoint from Asia. *Bull. Natl. Res. Cent.* **44**, 80 (2020).
8. Sen, S., Abdullah-Al-Shafi, M., Mubassera, M. & Hawlader, Md. T. H. A high-sensitivity photonic crystal fibre biosensor for malaria detection. *Sens. Bio-Sens. Res.* 100963 (2026) doi:10.1016/j.sbsr.2026.100963.

9. Nedoma, J. *et al.* Decade of advancements in light–matter interaction-based optical fiber biosensing: innovations, challenges, and future directions. *Adv. Photonics* **8**, 014004 (2025).

10. Sharma, D. S. *et al.* V-Grooved Gold-Coated Photonic Crystal Fiber Sensor for Sensitivity Analysis of Tumor Detection in the Near-Infrared Region. *Photonics Lett. Pol.* **17**, 42–44 (2025).

11. Sharma, S. *et al.* Design and Numerical Analysis of a Gold-Coated Photonic Crystal Fiber Sensor for Metabolic Disorder Detection with Deep Learning Assistance. *Plasmonics* **20**, 8923–8933 (2025).

12. Abdullah-Al-Shafi, Md. & Sen, S. Design and analysis of a chemical sensing octagonal photonic crystal fiber (O-PCF) based optical sensor with high relative sensitivity for terahertz (THz) regime. *Sens. Bio-Sens. Res.* **29**, 100372 (2020).

13. Hossain, Md. S. *et al.* Performance analysis of alcohols sensing with optical sensor procedure using circular photonic crystal fiber (C-PCF) in the terahertz regime. *Sens. Bio-Sens. Res.* **35**, 100469 (2022).

14. Sen, S., Abdullah-Al-Shafi, Md. & Kabir, M. A. Hexagonal photonic crystal Fiber (H-PCF) based optical sensor with high relative sensitivity and low confinement loss for terahertz (THz) regime. *Sens. Bio-Sens. Res.* **30**, 100377 (2020).

15. Britto, E. C., Krishnamoorthi, B., Rajasekar, R. & Nizar, S. M. Photonic Crystal–Based Nanoscale Multipurpose Biosensor for Detection of Brain Tumours, HIV, and Anaemia with High Sensitivity. *Plasmonics* **19**, 2687–2703 (2024).

16. Dinish, U. S., Beffara, F., Humbert, G., Auguste, J. & Olivo, M. Surface-enhanced Raman scattering-active photonic crystal fiber probe: Towards next generation liquid biopsy sensor with ultra high sensitivity. *J. Biophotonics* **12**, e201900027 (2019).

17. Soylemez, S. *et al.* Electrochemical and optical properties of a conducting polymer and its use in a novel biosensor for the detection of cholesterol. *Sens. Actuators B Chem.* **212**, 425–433 (2015).
18. Sun, D., Guo, T., Ran, Y., Huang, Y. & Guan, B.-O. In-situ DNA hybridization detection with a reflective microfiber grating biosensor. *Biosens. Bioelectron.* **61**, 541–546 (2014).
19. Saftawy, E. E. *et al.* Malaria: biochemical, physiological, diagnostic, and therapeutic updates. *PeerJ* **12**, e17084 (2024).
20. Mmileng, O. P., Whata, A., Olusanya, M. & Mhlongo, S. Application of ConvNeXt with transfer learning and data augmentation for malaria parasite detection in resource-limited settings using microscopic images. *PLOS ONE* **20**, e0313734 (2025).
21. Fikadu, M. & Ashenafi, E. Malaria: An Overview. *Infect. Drug Resist.* **Volume 16**, 3339–3347 (2023).
22. Leong, Y. W., Russell, B., Malleret, B. & Rénia, L. Erythrocyte tropism of malarial parasites: The reticulocyte appeal. *Front. Microbiol.* **13**, 1022828 (2022).
23. Abdullah-Al-Shafi, Md., Akter, N., Sen, S. & Hossain, Md. S. Design and performance analysis of background material of zeonex based high core power fraction and extremely low effective material loss of photonic crystal fiber in the terahertz (THz) wave pulse for many types of communication areas. *Optik* **243**, 167519 (2021).
24. Abdullah-Al-Shafi, Md. & Sen, S. Design of a low material loss and larger effective area based photonic crystal fiber for communication applications in terahertz (THz) waveguide. *Sens. Bio-Sens. Res.* **31**, 100400 (2021).
25. Mollah, M. S. H., Abdullah-Al-Shafi, Md., Hossain, Md. S. & Sen, S. An ultra-low material loss ellipse core-based photonic crystal fiber for terahertz wave guiding: design and analysis. *J. Comput. Electron.* **20**, 1541–1548 (2021).

26. Sen, S., Abdullah-Al-Shafi, Md., Sikder, A. S., Hossain, Md. S. & Azad, M. M. Zeonex based decagonal photonic crystal fiber (D-PCF) in the terahertz (THz) band for chemical sensing applications. *Sens. Bio-Sens. Res.* **31**, 100393 (2021).
27. Frosch, T., Knebl, A. & Frosch, T. Recent advances in nano-photonic techniques for pharmaceutical drug monitoring with emphasis on Raman spectroscopy. *Nanophotonics* **9**, 19–37 (2020).
28. Luo, W. *et al.* Terahertz Sensor via Ultralow-Loss Dispersion-Flattened Polymer Optical Fiber: Design and Analysis. *Materials* **14**, 4921 (2021).
29. Bendib, S. & C, B. Photonic Crystals for Malaria Detection. *J. Biosens. Bioelectron.* **09**, (2018).
30. Gul, B., Ashraf, S., Khan, S., Nisar, H. & Ahmad, I. Cell refractive index: Models, insights, applications and future perspectives. *Photodiagnosis Photodyn. Ther.* **33**, 102096 (2021).
31. Park, Y. *et al.* Refractive index maps and membrane dynamics of human red blood cells parasitized by *Plasmodium falciparum*. *Proc. Natl. Acad. Sci.* **105**, 13730–13735 (2008).
32. Amin, R. *et al.* GaAs-filled elliptical core-based hexagonal PCF with excellent optical properties for nonlinear optical applications. *Ceram. Int.* **48**, 5617–5625 (2022).
33. Zhao, J. *et al.* Pressure and temperature sensors based on an over-discharged spliced polarization-maintaining photonic crystal fiber. *Opt. Express* **32**, 30839 (2024).
34. Jabin, Md. A. *et al.* Surface Plasmon Resonance Based Titanium Coated Biosensor for Cancer Cell Detection. *IEEE Photonics J.* **11**, 1–10 (2019).
35. Ji, Y. *et al.* Dual-Core Photonic Crystal Fiber Polarization Beam Splitter Based on a Nematic Liquid Crystal with an Ultra-Short Length and Ultra-Wide Bandwidth. *Electronics* **13**, 2343 (2024).

36. Rao, X., Yang, L., Su, J. & Xie, H. Hardware-Described Nanoscale Carry-Save Adder in Quantum-Dot Cellular Automata: An Optimised Design and Evaluation Framework. *J. Light. Technol.* **42**, 6912–6924 (2024).
37. Khonina, S. N., Kazanskiy, N. L. & Butt, M. A. Optical Fibre-Based Sensors—An Assessment of Current Innovations. *Biosensors* **13**, 835 (2023).
38. Luo, X., Tsai, D., Gu, M. & Hong, M. Extraordinary optical fields in nanostructures: from sub-diffraction-limited optics to sensing and energy conversion. *Chem. Soc. Rev.* **48**, 2458–2494 (2019).
39. Islam, Md. S. *et al.* A Novel Approach for Spectroscopic Chemical Identification Using Photonic Crystal Fiber in the Terahertz Regime. *IEEE Sens. J.* **18**, 575–582 (2018).
40. Melati, D., Melloni, A. & Morichetti, F. Real photonic waveguides: guiding light through imperfections. *Adv. Opt. Photonics Vol 6 Issue 2 Pp 156-224* https://doi.org/10.1364/AOP.6.000156 (2014) doi:10.1364/AOP.6.000156.
41. Zhang, Y. *et al.* Advanced optical polarizers based on 2D materials. *Npj Nanophotonics* **1**, 28 (2024).
42. Chaudhary, V. S., Kumar, D. & Kumar, S. Gold-Immobilized Photonic Crystal Fiber-Based SPR Biosensor for Detection of Malaria Disease in Human Body. *IEEE Sens. J.* **21**, 17800–17807 (2021).
43. Ferdous, A. H. M. *et al.* Optical communications with guided wave fibers with rectangular cladding for fuel adulteration detection. *J. Opt. Commun.* **45**, (2023).
44. Habib, Md. A. *et al.* Efficient way for detection of alcohols using hollow core photonic crystal fiber sensor. *Opt. Rev.* **28**, 383–392 (2021).
45. Hossain, Md. S. & Sen, S. Design and Performance Improvement of Optical Chemical Sensor Based Photonic Crystal Fiber (PCF) in the Terahertz (THz) Wave Propagation. *Silicon* **13**, 3879–3887 (2021).

46. Iqbal, F. *et al.* Alcohol sensing and classification using PCF-based sensor. *Sens. Bio-Sens. Res.* **30**, 100384 (2020).

47. Jibon, R. H., Biswas, S., Biswas, S. & Nira, N. F. I. Poisonous chemical detection in the THz regime using PCF: Design and numerical investigation. *J. Opt.* **50**, 671–680 (2021).

48. Srivastava, R., Prajapati, Y. K., Pal, S. & Kumar, S. Micro-Channel Plasmon Sensor Based on a D-Shaped Photonic Crystal Fiber for Malaria Diagnosis With Improved Performance. *IEEE Sens. J.* **22**, 14834–14841 (2022).

49. Abdullah-Al-Shafi, M. & Sen, S. A Sophisticated Terahertz Photonic Crystal Fiber Sensor Design for Highly Accurate Detection of Kerosene Mixtures. *Adv. Phys. Res.* **4**, 2500025 (2025).

50. Abdullah-Al-Shafi, Md., Sen, S. & Mubassera, M. Insecure food additive sensing with photonic crystal fibre in terahertz regime. *J. Mod. Opt.* **71**, 762–770 (2024).

51. Butt, M. A., Mateos, X. & Piramidowicz, R. Photonics sensors: A perspective on current advancements, emerging challenges, and potential solutions (Invited). *Phys. Lett. A* **516**, 129633 (2024).

52. Sahana Bujugundla, R. & Pradhan, H. S. Emerging Technologies for Fiber-Optic-Based Sensors in Biomedical Domain: A Review and Recent Developments. *IEEE Trans. Instrum. Meas.* **73**, 1–32 (2024).

53. Sawraj, S. *et al.* PCF-Based Sensors for Biomedical Applications: A Review. *IEEE Trans. NanoBioscience* **24**, 157–164 (2025).

54. Sen, S. & Abdullah-Al-Shafi, M. Emphasis on sensitivity and accuracy: Design and optimization of a high-sensitivity terahertz photonic crystal fiber sensor for precision analysis of petrochemical-based adulterants in hydrocarbon mixtures. *Sens. Bio-Sens. Res.* **49**, 100823 (2025).

55. Sharif, V., Saberi, H. & Pakarzadeh, H. Designing a terahertz optical sensor based on helically twisted photonic crystal fiber for toxic gas sensing. *Sci. Rep.* **15**, 2268 (2025).

56. Vettoruzzo, A., Bouguelia, M.-R., Vanschoren, J., Rögnvaldsson, T. & Santosh, K. Advances and Challenges in Meta-Learning: A Technical Review. *IEEE Trans. Pattern Anal. Mach. Intell.* **46**, 4763–4779 (2024).
57. Zhang, Y. *et al.* GAN-MAML strategy for biomass energy production: Overcoming small dataset limitations. *Appl. Energy* **387**, 125568 (2025).
58. Long, J. *et al.* A Comprehensive Review of Signal Processing and Machine Learning Technologies for UHF PD Detection and Diagnosis (II): Pattern Recognition Approaches. *IEEE Access* **12**, 29850–29890 (2024).
59. Demiss, B. A. & Elsaigh, W. A. Application of novel hybrid deep learning architectures combining Convolutional Neural Networks (CNN) and Recurrent Neural Networks (RNN): construction duration estimates prediction considering preconstruction uncertainties. *Eng. Res. Express* **6**, 032102 (2024).
60. Kumar, S., Arif, T., Alotaibi, A. S., Malik, M. B. & Manhas, J. Advances Towards Automatic Detection and Classification of Parasites Microscopic Images Using Deep Convolutional Neural Network: Methods, Models and Research Directions. *Arch. Comput. Methods Eng.* **30**, 2013–2039 (2023).
61. Kornaros, G. Hardware-Assisted Machine Learning in Resource-Constrained IoT Environments for Security: Review and Future Prospective. *IEEE Access* **10**, 58603–58622 (2022).
62. Wong, F., De La Fuente-Nunez, C. & Collins, J. J. Leveraging artificial intelligence in the fight against infectious diseases. *Science* **381**, 164–170 (2023).